Journal of Power Sources 196 (2011) 7665–7672

Contents lists available at ScienceDirect

Journal of Power Sources

journal homepage: www.elsevier.com/locate/jpowsour

A prefilter for mitigating PH_3 contamination of a Ni-YSZ anode

Chunchuan Xu[a,*], John W. Zondlo[a], Edward M. Sabolsky[b]

[a] Department of Chemical Engineering, West Virginia University, Morgantown, WV 26506, USA
[b] Department of Mechanical & Aerospace Engineering, West Virginia University, Morgantown, WV 26506, USA

ARTICLE INFO

Article history:
Received 14 February 2011
Received in revised form 21 April 2011
Accepted 22 April 2011
Available online 30 April 2011

Keywords:
SOFC
Ni-YSZ anode
Coal-syngas
Phosphine
Phosphine removal filter

ABSTRACT

Ni-YSZ is used as the anode of a solid oxide fuel cell (SOFC) because it has excellent electrochemical performance for operation with coal-derived syngas. However, trace impurities, PH_3 H_2S AsH_3, and Sb in coal-syngas can cause SOFC degradation. Described here is a means of removing PH_3 impurity from syngas by using a Ni-based prefilter. In one test, a thin Ni-based filter was set upstream of a Ni-YSZ anode-supported SOFC. The SOFC was exposed to syngas with PH_3 under a constant current load at 800 °C. The filter decreased 20 ppm PH_3 in the feed to a level which did not degrade the SOFC for over 400 h until the filter became saturated. In another test, both H_2S and PH_3 were co-fed to the cell with Ni-based and Fe/Ni-based filters. The interaction between these two impurities did not significantly impact the filter performance with respect to PH_3 removal for both filter formulations. The cell performance was evaluated by current–voltage measurements and impedance spectroscopy. Post-mortem analyses of the cell and filter were performed by means of XRD, SEM/EDS and XPS. With proper filter design, the Ni-YSZ SOFC can operate on contaminated coal-syngas without degradation over a prescribed period of time.

1. Introduction

The poisoning effect of PH_3 on a Ni-YSZ anode-supported cell using synthesized snygas and hydrogen fuel has been investigated under various operating conditions in previous papers [1,2]. Previous work showed that the degradation rate of a Ni-YSZ anode-supported cell is 0.5–1.0 mV h^{-1} upon exposure to syngas with 10 ppm PH_3 at 800 °C. Nickel phosphide compounds were identified as products on the Ni-YSZ anode surface. Similar poisoning effects of PH_3 in syngas mixtures and H_2 fuel on Ni-YSZ anodes were reported by other investigators [3,4]. It is clear that the degradation of the Ni-YSZ anode-supported SOFC results not only in the formation of nickel phosphide compounds but also with significant reconstruction of the Ni-YSZ anode if parts per million levels of PH_3 impurity reach the anode at typical SOFC operating conditions.

In this work, the capability of various filters for PH_3 removal has been evaluated by using Ni-YSZ anode-supported SOFC's. At first, a Ni-based filter upstream of the cell was exposed to syngas with PH_3 impurity and assessed for PH_3 removal. Then iron was added as the active filter material and both the Fe-based and Fe/Ni-based (iron mixed with nickel as the active filter material) filters were tested. Both the Ni-based and Fe/Ni-based filters were operated with 20 ppm H_2S and 20 ppm PH_3 binary impurities in syngas fuel. Periodic evaluation of the impedance assessed the ohmic and polarization resistances during the experiments. Extensive post-mortem analyses by SEM, XRD and XPS allowed evaluation of the chemical and microstructure changes in the both the spent filter and the anode. These results are discussed and compared to previous poisoning studies with PH_3 impurity.

2. Experimental methods

2.1. SOFC and test setup

Commercial anode-supported solid oxide button cells manufactured by Materials and Systems Research Inc. (MSRI) were used. A detailed description of the cell composition, structure, dimensions and cell contact configuration has been reported in a previous paper [1]. Mass flow controllers were employed to control the flow rates of H_2, CO, CO_2, N_2/PH_3 (1000 ppm PH_3 in a balance of nitrogen), N_2/H_2S (1000 ppm H_2S in a balance of nitrogen) and air separately. A temperature-controlled humidifier was used to adjust the H_2O concentration of the simulated coal syngas fed to the anode. The syngas (32% H_2, 18% H_2O, 31% CO and 19% CO_2) flow rate was kept constant at approximately 200 standard cubic centimeters per minute (sccm). The air-flow rate to the cathode was held at approximately 300 sccm. The overall test setup was described in a previous paper [2]. The filter is a porous pellet and is composed of nickel, iron or a mixture of nickel and iron.

* Corresponding author at: Department of Chemical Engineering, West Virginia University, Morgantown, WV 26506-6012, USA. Tel.: +1 304 293 9379; fax: +1 304 293 4139.
E-mail address: Chunchuan.Xu@mail.wvu.edu (C. Xu).

0378-7753/$ – see front matter © 2011 Elsevier B.V. All rights reserved.
doi:10.1016/j.jpowsour.2011.04.054

2.2. Electrochemical testing of the SOFC

The tests followed the same procedure that was described in previous work [1] except that the filter was installed immediately upstream of the cell. To investigate the PH_3 removal, the cell OCV, voltage under 0.5 A cm^{-2} load and degradation rates for all the tests have been recorded. Impedance spectra were taken periodically during cell testing using a Solartron SI 1260 impedance/gain-phase analyzer with AC amplitude of 20 mV at frequencies ranging from 200 kHz to 0.1 Hz. To inspect whether or not the PH_3, H_2S or both impurities passed through the filter to cause cell degradation, the cell voltage under constant-current load was recorded every 20 s. After each cell test was completed, the anode side was purged with 80% N_2 and 20% H_2 while being cooled to room temperature in about 4 h. This purge minimized the exposure of the cell anode to ambient air.

2.3. Morphology, chemical and thermodynamic analyses

The microstructure and chemical composition of the cell anode were examined with a Hitachi S-4700 SEM/EDS. To determine the composition of the anode, an XRD (Panalytical X'Pert Pro PM-3040) with a Cu K-alpha radiation source (1.54060 Å), and an XPS (PHI 5000 VerasProbe XPS Microprobe) with a monochromatic Al K-alpha radiation source (8.34118 Å) were employed. Thermodynamic analysis was carried out with the FACTSAGE 5.4 software package.

3. Experimental results

3.1. Ni-based filter test

The Ni-based filter-1 was installed immediately upstream of the cell anode and sealed around its edge by a tiny amount of nickel paste. The cell and filter-1 were loaded in the test stand simultaneously. After accounting for a slight change in cell performance during the initial break-in period at constant current density of 0.5 A cm^{-2}, the cell voltage under load was stable at 0.710 V over 60 h in coal syngas (Fig. 1, period (a)). Following the introduction of 10 ppm PH_3, the cell performance quickly starts to degrade by about 10 mV in 40 h. Then the cell voltage remained stable at 0.700 V for 200 h (Fig. 1, period (b)). Compared to the cell at the same conditions without a filter [1], the cell would lose about 100–200 mV over this same time period. The cell was cooled to room temperature and the filter-1 was easily disassembled from the cell and removed for examination. The cell was reloaded in the test stand without the filter and tested in the clean syngas fuel at 800 °C for the next 50 h whereupon the cell performance slightly recovered by about 6 mV (Fig. 1, period (c)). Then the cell was cooled to room temperature for installation of filter-2 which was identical to filter-1. After the cell was reloaded and operated for about 30 h in the clean syngas (Fig. 1, period (d)), 20 ppm PH_3 was injected upstream in the syngas. The cell voltage dropped about 30 mV in the initial 20 h, and then it slowly increased by 15 mV in the following 150 h. The cell voltage remained at about 0.685 V during the test. After exposure of the cell with filter-2 to 20 ppm PH_3 for 400 h, a power failure interrupted the test for about 30 h. When the cell was brought back to the previous testing conditions, it started to slowly lose its performance. In the next 200 h, the cell voltage dropped by about 30 mV. The overall loss of the cell voltage is about 45 mV in period (e). Significant cell degradation started in the last 200 h after the power failure. After finishing the test, the cell was cooled to room temperature by purging with 20% H_2 and 80% N_2 to prevent oxidation of the cell anode. Filter-2 was severely reconstructed and fused on to the cell anode as shown in Fig. 5. The 20 ppm PH_3 penetrated through the filter-2 and started to attack the cell. The PH_3 break through front position is indicated on the cell anode by the arrow in Fig. 5b.

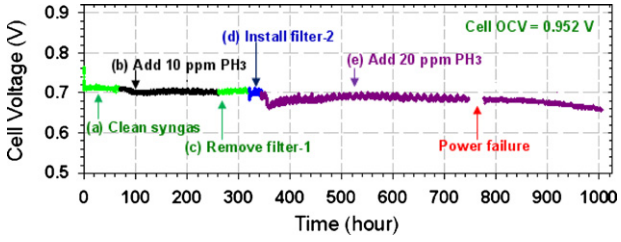

Fig. 1. The cell voltage versus time during the entire 1000 h test. The cell started to lose voltage in the last 200 h after a power failure. The PH_3 removal filter-2 was found completely saturated by the 20 ppm PH_3.

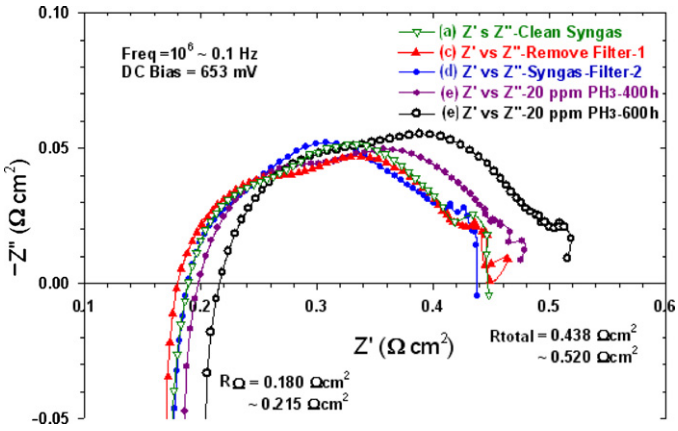

Fig. 2. The cell impedance spectra in 5 different phases of the 1000 h test. The ohmic and polarization resistances increased significantly during phase (e), the cell exposed to 20 ppm PH_3 between 400 h and 600 h.

The impedance spectra under a DC bias of 653 mV show that the ohmic resistance (high frequency intercept with the Z' axis) and the total polarization resistance (low frequency intercept with Z' axis) both mildly increase with increasing time of exposure to PH_3. The impedance spectra at the end of periods (a), (c), (e) before power failure (PH_3 for 400 h) and the end of (e) (PH_3 for 600 h) are shown in Fig. 2. The area specific ohmic resistance, R_Ω, did not show significant changes from its value of $0.195 \pm 0.010\ \Omega\ cm^2$. The total polarization resistances also remained constant at $R_\rho = 0.261 \pm 0.012\ \Omega\ cm^2$. After adding 20 ppm PH_3 for about 400 h in period (e), the ohmic resistance, R_Ω, and the polarization resistance, R_ρ, slightly increased by about 0.01 $\Omega\ cm^2$ and 0.012 $\Omega\ cm^2$, respectively. The significant change of the ohmic resistance R_Ω and the total cell resistance R_{total} occurred between 400 h and 600 h exposure to 20 ppm PH_3 when the phosphine broke through the filter.

Post-mortem photographs of filter-1 are shown in Fig. 3. The front surface of the filter (Fig. 3a) which faced the syngas with 10 ppm PH_3 was reconstructed. The XRD spectrum of the filter's front surface indicates that Ni_5P_2 was built up on this surface (Fig. 4a). The XRD spectrum of the backside surface (image in Fig. 3b) of filter-1 did not show any detectable nickel phosphide (Ni_5P_2) signals in Fig. 4b [1]. This evidence explains why the cell was protected from PH_3 attack by filter-1 during the 200 h of testing. PH_3 impurity did not penetrate filter-1 with a high enough threshold concentration to react with the nickel in the anode and produce nickel phosphide. The cell was also tested subsequently in syngas without any filter or PH_3 and showed no significant degradation in performance. The cell voltage did not significantly

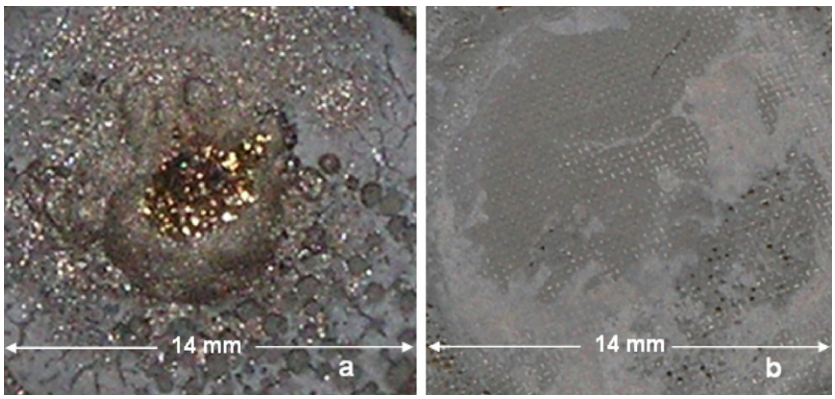

Fig. 3. A photograph of the front face of filter-1 which was exposed to syngas with 10 ppm PH_3 for 200 h (a) and (b) backside of the same filter.

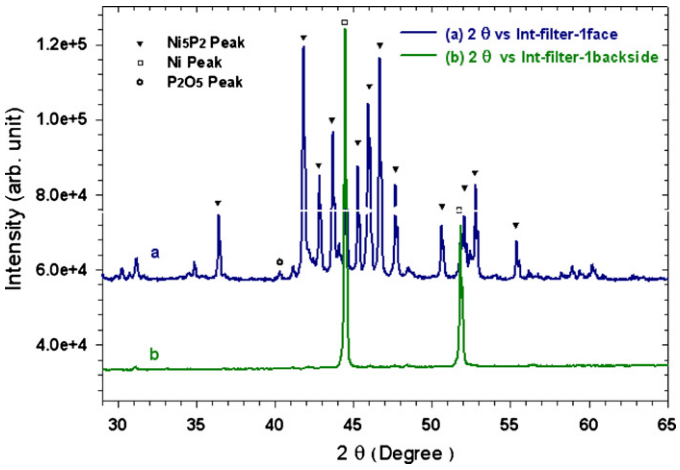

Fig. 4. XRD sepctra of the PH_3 poisoned filter-1 (a) exposed surface and (b) backside.

change after the installation of filter-2. The image of the poisoned filter-2 in Fig. 5 showed that more severe structural reconstruction occurred on filter-2 than on filter-1. Nickel particles less than 10 μm have grown to over 1000 μm and formed nickel phosphide in the center of filter-2. The EDS spectrum of the cross-section of filter-2 (Fig. 6a) indicted that the P signal appeared through the entire cross-section. The top surface structure of the Ni-YSZ anode showed evidence of PH_3 attack, indicating PH_3 breakthrough of the filter. This observation agrees with the loss of cell performance after exposing the cell/filter-2 assembly to 20 ppm PH_3 for 600 h.

3.2. Fe-based filter test

A fresh SOFC from the same batch of those previously tested was loaded in the test stand, this time with an Fe-based filter ahead of it. After the cell had operated for 50 h in clean syngas under a load of 0.5 A cm^{-2} at 800 °C, the cell voltage stabilized at about 0.680 V. Then 20 ppm PH_3 was injected into the syngas. During the next 215 h, the cell voltage slowly dropped at a rate of about 0.13 mV h^{-1} resulting in a total loss of voltage of 30 mV (Fig. 7). The impedance spectra before and after adding 20 ppm PH_3 for 215 h showed that the ohmic resistance R_Ω stayed constant at 0.205 Ω cm^2, and only the polarization resistance increased slightly (Fig. 8). After the cell with the Fe-based filter was cooled, the filter was examined. A dense layer formed on the surface of the Fe-based filter which can be seen clearly in Fig. 9a. The cross-sectional image of the filter showed that the dense layer is about 150 μm thick and is localized on the top surface of the Fe-based filter (Fig. 9b). The EDS spectrum of this dense layer reveals that Fe, P and O are the major components in the layer (Fig. 6b). The strong oxygen signal implies that ferrous phosphate was produced on the Fe-based filter surface.

3.3. Cross-poisoning of H_2S and PH_3 impurities

To investigate any possible interaction between the two poisons, H_2S and PH_3, on the filter and Ni-YSZ anode, a fresh cell with different filters was tested with 0.5 A cm^{-2} constant current density for about 1100 h as shown in Fig. 10. During phase-(a) (see Fig. 10), the cell with the Ni-based filter-3 was fed clean syngas for 150 h. Subsequently 20 ppm H_2S was added to the syngas in phase-(b) for 75 h. The cell voltage remained constant at 0.710 V for about 25 h, and then quickly dropped 35 mV in the next 15 h following the H_2S

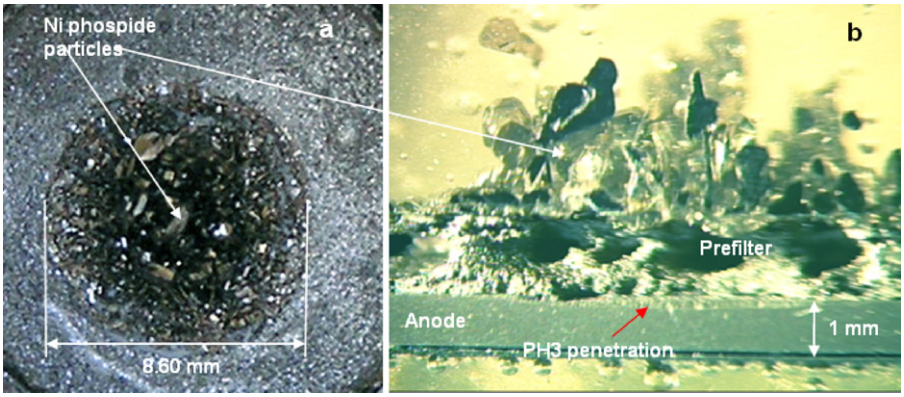

Fig. 5. The images of the central area of (a) the filter-2 surface and (b) the cell with filter-2 cross-section. 20 ppm PH_3 penetrated the filter-2 and attacked the cell anode top surface.

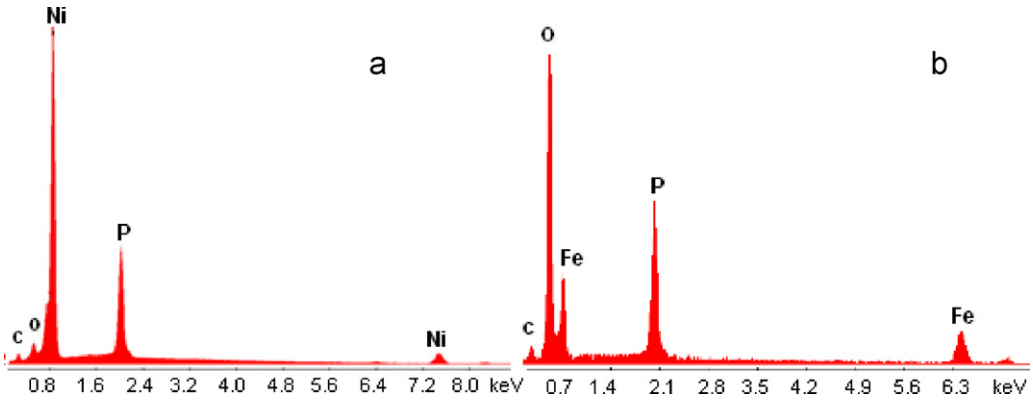

Fig. 6. The EDS spectra of the PH_3 poisoned surface of (a) the Ni-based filter-2 and (b) the Fe-based filter. The strong oxygen peak appeared on the PH_3 poisoned Fe-based filter but not on the PH_3 poisoned Ni-based filter.

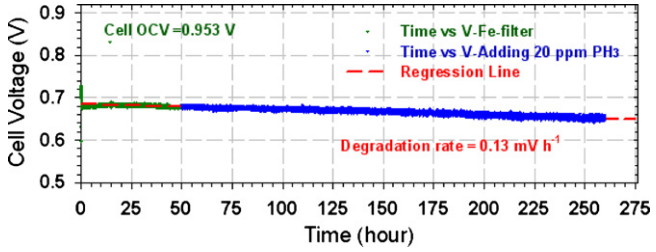

Fig. 7. The voltage versus time of the cell with the Fe-based filter exposed to 20 ppm PH_3 in syngas for 215 h.

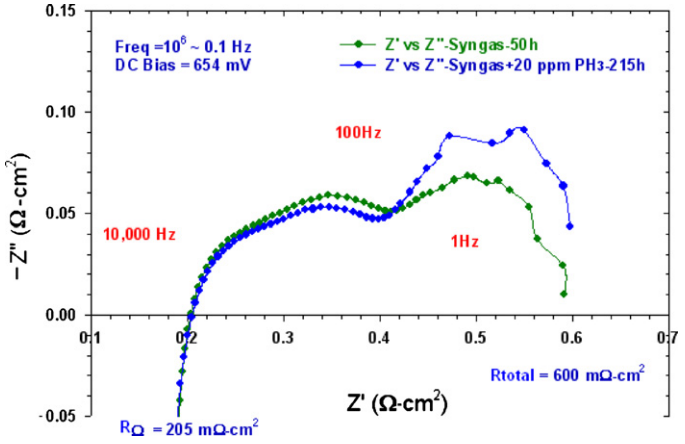

Fig. 8. The impedance spectra of the cell with the Fe-based filter exposed to 20 ppm PH_3 in syngas.

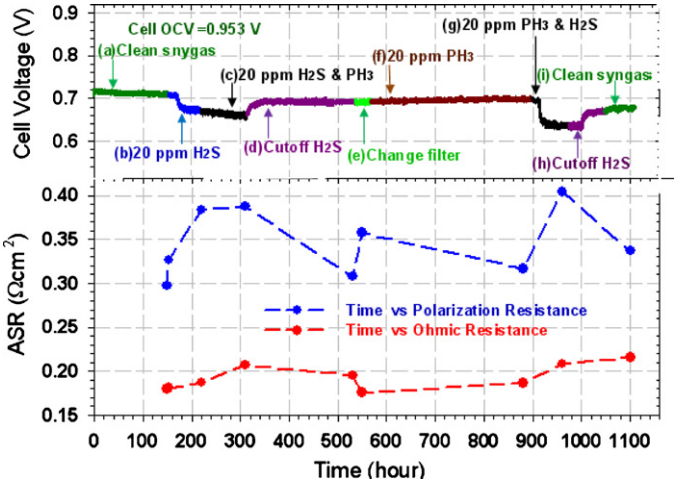

Fig. 10. The cell voltage and area specific resistance versus time during the entire 1100 h test. The cell ohmic resistance remained almost constant and the polarization resistance increased when 20 ppm H_2S was added to the fuel.

addition. After that, the cell slowly lost voltage at a degradation rate of 0.126 mV h^{-1} in the subsequent 30 h. In phase-(c), an additional 20 ppm PH_3 impurity was injected into syngas fuel. The cell showed almost the same degradation rate for the next 100 h. After 20 ppm H_2S impurity was cut off, the cell voltage rapidly recovered to 0.690 V and remained at this level of performance for 200 h as indicated in phase-(d). This implies that the filter can block the poisoning caused by PH_3, but H_2S still penetrated the filter-3 to attack

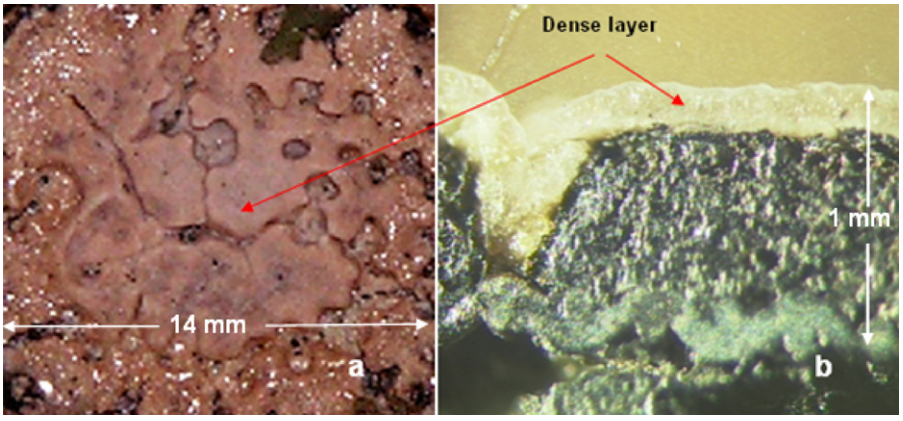

Fig. 9. A photograph of the Fe-based filter (a) the PH3 piosoned surface (b) the cross-section under 25× magnification.

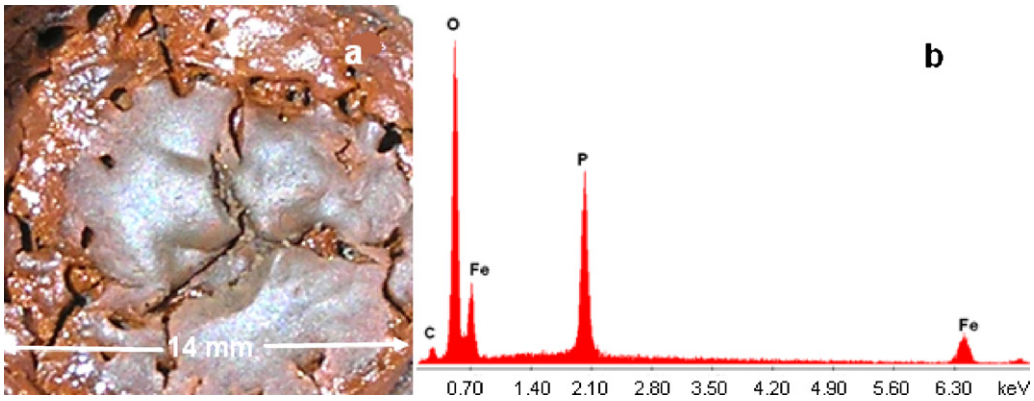

Fig. 11. (a) The image of the poisoned Fe/Ni-based filter surface. The ferrous phosphate layer exhibits a cracked and porous structure. (b) The EDS spectrum of the poisoned Fe/Ni-based filter surface.

the cell. The cell was cooled to room temperature and filter-3 was inspected. The filter's center surface showed a build up of nickel phosphide particles similar to the image of filter-2 in Fig. 5. The back side of the filter which faced the cell anode was clean nickel with no formation of nickel phosphides.

3.4. Iron/nickel-based filter test

After removing filter-3 at the end of phase-(d) (Fig. 10), the cell was reloaded and fed with clean syngas for 30 h in phase-(e). The cell performance was slightly higher by about 3–5 mV than that seen in phase-(d). Then the cell was cooled to room temperature and another filter was installed. This filter version was a combination of iron and nickel (Fe/Ni-based). The cell combined with the Fe/Ni-based filter was reloaded and stabilized in clean syngas. Sequentially 20 ppm PH_3 impurity was injected into the syngas fuel. Rather than degrading, the cell performance continually increased by about 10 mV for 320 h in phase-(f). This suggests that Fe/Ni-based filter may be more effective at PH_3 removal than the purely Ni-based filter. To examine the H_2S impurity poisoning effect on the cell with the Fe/Ni-based filter, an additional 20 ppm H_2S was loaded in the fuel. The cell quickly lost voltage during the first 16 h under the 20 ppm H_2S loading. After quickly dropping 50 mV, the cell voltage degradation rate decreased to as low as 0.06 mV h^{-1} which is half that seen when the Ni-based filter was used in phase-(g). Although the Fe/Ni-based filter cannot remove H_2S completely, it did reduce the H_2S poisoning more effectively than the Ni-based filter. After cutting off the H_2S in phase-(h), the cell voltage did not recover until it quickly increased by about 30 mV after 20 h. Then the cell voltage slowly returned to 0.670 V for about 40 h. When the PH_3 flow was stopped, the cell continually recovered another 10 mV with clean syngas fuel in phase-(i) for the next 60 h until the end of the test. The electrochemical impedance spectra were recorded at each of the different phases. The area specific ohmic resistance and polarization resistance are plotted against cell voltage versus time in Fig. 10. The ohmic resistance did not show a significant increasing trend during the entire 1100 h test if the measurement errors is taken into account, i.e., $R_\Omega = 0.193 \pm 0.014\ \Omega\ cm^2$. The polarization resistance slightly increased by about 0.08 Ωcm^2 when 20 ppm H_2S impurity was added.

An image of the poisoned Fe/Ni-based filter is shown in Fig. 11a. The filter surface was severely altered both in structure and color. In comparison to the poisoned Fe-based filter in Fig. 9a, the poisoned Fe/Ni-based filter surface exhibited many open holes and cracks

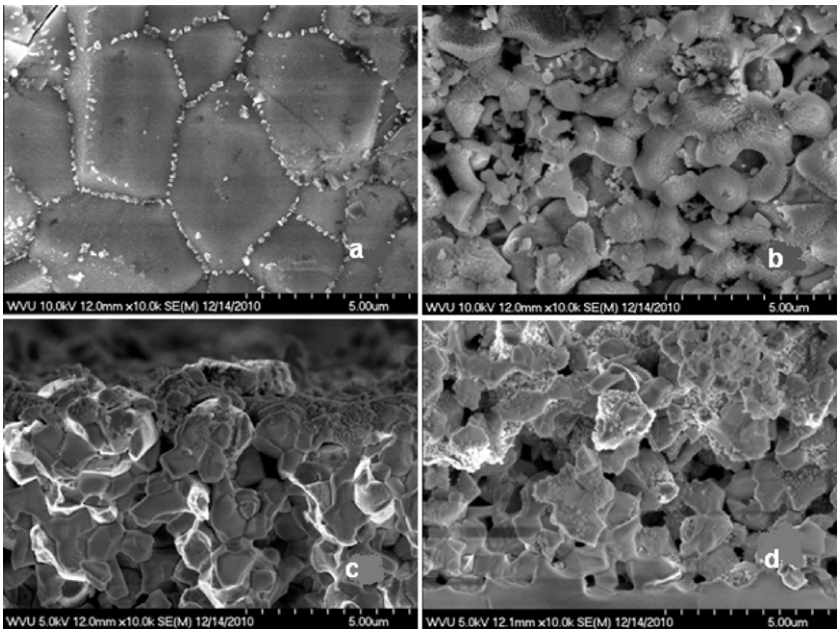

Fig. 12. SEM images of (a) the poisoned Fe/Ni-based filter surface, (b) the cell anode surface, (c) the anode cross-section near the top of the anode and (d) the anode active layer near the electrolyte.

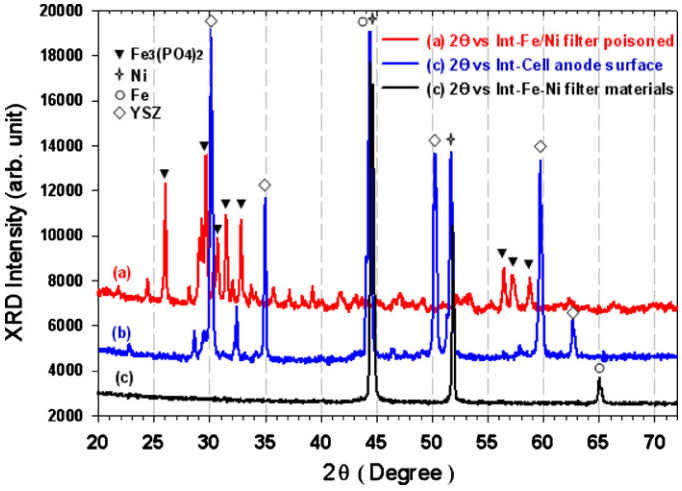

Fig. 13. The XRD spectra of (a) 20 ppm PH_3 poisoned Fe/Ni-based filter and (b) the cell anode surface (c) the unreacted (clean) Fe/Ni-based filter.

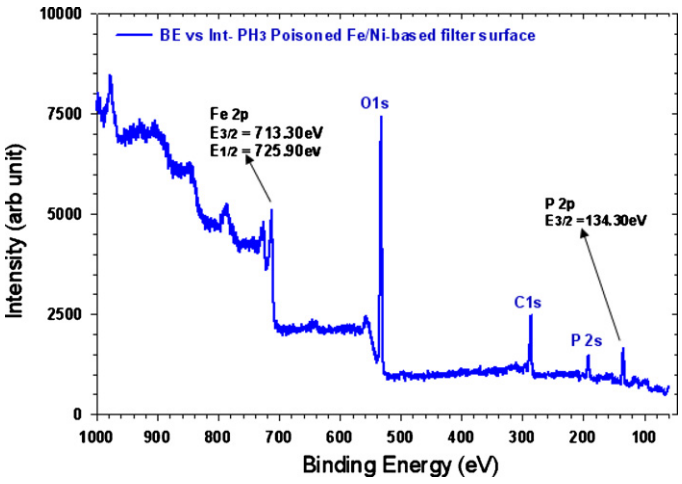

Fig. 14. XPS spectrum of the PH_3-poisoned Fe/Ni-based filter surface.

which allowed fuel flow through it. The EDS spectrum of this surface identified that phosphorus, iron and oxygen are the main species on the poisoned filter surface. The SEM image in Fig. 12a indicates that the microstructure of the poisoned filter surface is very dense with sealed grain boundaries. Compared to the SEM image of the cell anode surface in Fig. 12b, the cell anode surface is porous with nickel and YSZ grains still intact and similar to a freshly reduced cell. The microstructure of the cell anode cross-section is displayed in Fig. 12c and d at different positions in the anode. There are no significant changes in structure at the top of the anode in Fig. 12c and at the anode active layer in Fig. 12d. There were a series of SEM images of the PH_3-poisoned and fresh Ni-YSZ anode in the previous work that can verify these observations [12].

The XRD spectrum of the poisoned Fe/Ni-based filter surface suggests that iron in the Fe/Ni-based filter reacted with PH_3 and H_2O to produce ferrous phosphate which agrees with the results of the EDS examination. $Fe_3(PO_4)_2$ is a dominant product shown in Fig. 13a [5]. There are no significant signals of nickel or nickel phosphide on the poisoned Fe/Ni-based filter. The spectrum of the clean Fe/Ni-based filter clearly displayed both iron and nickel peaks in Fig. 13c [6,7]. This evidence suggests that the iron reacts more favorably with PH_3 under SOFC working conditions. The XRD spectrum of the cell anode basically displayed Ni-YSZ peaks in Fig. 13b [8]. There are no nickel phosphide signals present indicating that PH_3 did not reach the cell surface. All peak identifications versus 2θ are listed in Table 1.

The XPS examination of the Fe/Ni-based filter surface provides information on the oxidation state of phosphorus and iron. The significant peaks in the XPS spectrum shown in Fig. 14 are phosphorus, iron, oxygen and carbon. There are no nickel peaks in the spectrum. These peaks should have appeared since nickel is present in the mixed filter. This observation may be a result of the different chemistry between the reaction of PH_3 with iron and nickel. From the detailed XPS scan of phosphorus 2p 3/2 peak at 134.60 eV, it is evident that the phosphate compound rather than the phosphide compound has been produced on the filter surface (Fig. 15a) [9]. And iron 2p 1/2 and 2p 3/2 peaks are at 713.30 eV and 725.90 eV which correspond to iron in the oxidation state found in ferrous phosphate $Fe_3(PO_4)_2$ [10].

Table 1
XRD peak list $2\theta^\circ$.

$Fe_3(PO_4)_2$ [5]	Fe [6]	Ni [7]	YSZ [8]
26.06°	44.65°	44.50°	30.10°
29.68°	65.01°	51.87°	34.89°
30.70°	82.31°		50.21°
31.53°			59.79°
32.82°			62.86°
53.41°			
56.46°			
57.21°			
58.79°			

The cell has been tested in syngas containing 20 ppm PH_3 impurity for about 730 h, and 20 ppm H_2S impurity for about 240 h. The total loss of the cell voltage under 0.5 A cm^{-2} load is about 40 mV. This loss of the cell voltage is predominantly caused by exposure to the H_2S impurity. The Fe/Ni filter was not penetrated by PH_3 over this time period. The removal of PH_3 by the filters was not impeded by the 20 ppm H_2S impurity.

4. Discussion

The main purpose of the filter is to reduce the PH_3 concentration down to a level which does not directly react with nickel in the Ni-YSZ anode. In both the Ni-based filter-1 and filter-2 tests, the cell lost about 10 and 30 mV, respectively, in the initial several hours after PH_3 injection, and then the cell voltage stabilized. This implies that phosphorus with a certain concentration level still reached to the cell interface causing the cell voltage to drop, the higher the concentration of PH_3 fed, the larger the voltage loss. This is remarkably similar to the initial poisoning effect reported for H_2S [11]. This initial poisoning effect of PH_3 has not been observed separately in tests of the bare cell without the filter because the continued feeding of a relatively high PH_3 concentration (over 1 ppm level) leads to rapid anode degradation by nickel phosphide formation. The poisoning behavior observed here can be explained by adsorption of phosphorus on nickel particles at the electrolyte/anode active layer which blocks hydrogen adsorption and the electrochemically active sites. Marina et al. [4] showed evidence of the presence of a phosphorus-containing surface adsorption layer within the nickel anode by ToF-SIMS. The oxidized phosphorus traces were identified on the post-mortem cells exposed to 10 ppm PH_3 at the anode active layer by XPS in a previous paper [2]. Thermodynamic calculations predicted that the formation of the first binary nickel phosphide phase is possible at phosphorus concentrations <1 ppb in coal gas at typical fuel cell operating temperatures [4]. For the Fe-based and Fe/Ni based filter tests, there is no significant loss of cell voltage in the initial phase with 20 ppm PH_3 as compared to the Ni-based filter case. This implies that iron could be a more efficient material than nickel for the removal of PH_3. Even though the concentration of the PH_3 after the filter was not measured

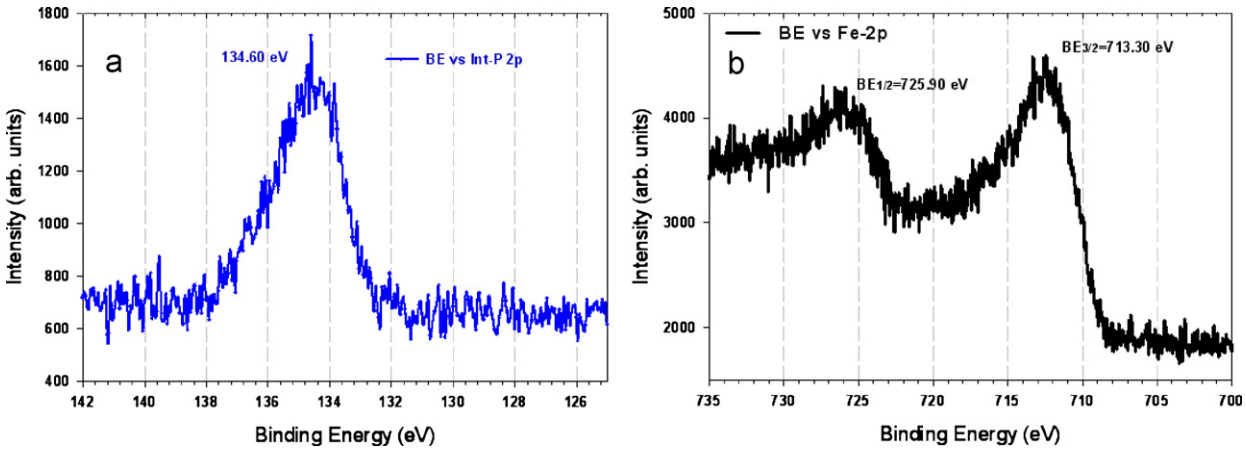

Fig. 15. The detailed XPS spectra of oxidation state P 2p 3/2 and Fe 2p 1/2, 3/2 peaks. The peak positions were calibrated according to the standard C1s position at 284.80 eV.

in situ, it can be expected that the filters did reduce the 20 ppm PH_3 below the threshold level required for the formation of nickel phosphide.

Both sulfur and phosphorus prefer the 4-fold step site adsorption structure of the nickel surface, and P–Ni bonding has more covalent character than the S–Ni bond. Phosphorus induces local reconstruction to make more favorable adsorption sites [12,13]. In the Ni-based filter-3 and Fe/Ni-based filter tests with 20 ppm H_2S included in the syngas along with 20 ppm PH_3, the cell degradation was always dominated the H_2S poisoning. The only possible explanation would be the PH_3 concentration was far below 20 ppm. PH_3 was almost completely removed by the nickel or iron in the filter and H_2S passed through the filter to interact with the anode active layer. The presence of H_2S does not interfere with the PH_3 removal in the filter. This is actually a fortuitous feature of the filter because a certain level H_2S would always be present in syngas and it could be dealt with after PH_3 removal or by using a sulfur-resistant anode.

Iron is a more cost-effective material than nickel. From the experimental observation of the Fe-based and Fe-/Ni-based filters, iron is more active when reacting with PH_3 forming ferrous phosphate ($Fe_3(PO4)_2$) under SOFC working conditions. But the ferrous phosphate tends to sinter and eventually blocks the fuel diffusion channels for the purely Fe-based filter. The cell lost performance not because of PH_3 poisoning but the diminished fuel transport which increases the diffusion polarization. For the Ni/Fe-based filter, nickel played the role of disassembling the ferrous phosphate agglomeration while simultaneously reacting with PH_3 to form nickel phosphide. Thus the Fe/Ni-based filter prevented PH_3 from attacking the cell for several hundred hours. There may be other cheaper materials that behave similarly to nickel in this regard. These substitutions will be investigated in future experiments.

Thermodynamic calculation showed that nickel phosphide Ni_5P_2 can be produced when nickel reacts with PH_3 under SOFC working conditions with $\Delta G = -247.5\,kJ\,mol^{-1}$ (1 mol PH_3) [12]. From previous work, nickel reacted with PH_3 in syngas to produce nickel phosphide compounds which are shiny and metallic gray in color. The poisoned Fe/Ni-based filter surface is a pink and lava-like compound. The XPS spectra of the Fe/Ni-based filter showed only one phosphorus 2p peak at 134.60 eV which is phosphorus in the PO_4^{3+} oxidation state. This is different from the case of PH_3 in syngas attacking nickel where phosphorus in the unoxidized state also appeared at 129.8 eV in the spectrum [2]. EDS and XRD characterization of the poisoned Fe/Ni-base filter also support the formation of ferrous phosphate. Thermodynamic calculation suggests that ferrous phosphate can be produced from a Fe/Ni-based filter under SOFC working conditions [14]. The absence of any nickel signals on the poisoned filter surface implies that iron preferentially migrated to the filter surface when it reacted with PH_3 and that iron is a more active filter material for PH_3 than nickel.

The prototype filters used in these experiments were about 1 mm thick with a surface area of 3 cm^2. For a filter 10 mm thick with comparable filter surface area, the lifetime of the filter can be extended to over several thousand hours. Additionally, the concentration of PH_3 is lower than 2 ppm in real coal syngas. This implies that the lifetime of such a filter can be expected to be over 10,000 h conservatively. Theoretically, the mass efficiency of the filter can be predicted. Assuming the product of nickel and PH_3 in the Ni-based filter is Ni_5P_2, 5 mol (140 g) nickel could remove 2 mol (18 g) PH_3 which is contained in 10^6 mol of syngas (syngas with 2 ppm PH_3). If the average molecular weight of syngas is 25 g mol^{-1}, the mass of 10^6 mole of syngas is 25 tons. So 140 g nickel could clean 25 tons of syngas at the 2 ppm PH_3 level. For the Fe/Ni-based filter, $Fe_3(PO_4)_2$ is the final product on the filter and the removal efficiency will be 1.6 times higher. The nickel phosphide and ferrous phosphate products can be subsequently recycled, disposed of, or regenerated.

Other trace impurities, such as arsine (AsH_3) and antimony Sb, also appear in real coal-derived syngas at levels lower than 1 ppm [15]. Because arsenic and antimony are in group V as is phosphorus, they should have similar chemistry when they interact with Ni on the Ni-YSZ anode [16–18]. So such a filter should remove AsH_3 and Sb as well. It is possible that the filter could be fabricated so that most of the severe nickel poisons in coal-derived syngas can be removed down to levels which can be tolerated by the SOFC.

5. Conclusion

A series of long-term tests of a Ni-YSZ anode-supported SOFC cell in tandem with filters for PH_3 removal exposed to syngas with 10 and 20 ppm PH_3 impurity has been evaluated. The 20 ppm PH_3 in syngas is highly favored to react with the nickel and iron in the filters to produce nickel phosphide and ferrous phosphate. By so doing, the PH_3 concentration is effectively reduced to levels which are not harmful to the Ni-YSZ anode. This behavior was observed for over several hundred hours until the filters became saturated by 20 ppm PH_3. The filtering effect occurs independently of the presence of H_2S in the syngas fuel. An initial limited loss of cell voltage caused by the adsorption of phosphorus on the Ni-YSZ anode has been observed under exposure to very low PH_3 concentrations. Iron is a cost-effective material for efficient PH_3 removal, but the sintered ferrous phosphate layer can block the fuel diffusion channels and reduce fuel transport. The addition of nickel to the iron-based filter was shown to inhibit the formation of the coherent iron product layer thus maintaining a porous structure

in the filter. From the experimental observation, iron is a better filter material for PH_3 removal than nickel. Thus the incorporation of such a filter upstream of the SOFC can be a simple and effective way of enhancing the useful lifetime of the fuel cell in syngas.

Acknowledgements

This work is conducted under US DOE (Department of Energy) EPSCoR Program. It is jointly sponsored by US DOE Office of Basic Energy Sciences, NETL (National Energy Technology Laboratory), WV State EPSCoR Office and the West Virginia University under grant number DE-FG02-06ER46299. Dr. Tim Fitzsimmons is the DOE Technical Monitor. Dr. R. Bajura is the Administrative Manager and Dr. I. Celik is the Technical Manager and Principal Investigator of this project. Dr. Kirk Gerdes, Dr. Greg Hackett, Dr. Hui Zhang, Liviu Magean and Adrienne MacLeod are thanked for thermodynamic calculation, taking the XPS, SEM, and EDS data. The results presented here have formed the basis of a pending patent application.

References

[1] C. Xu, J. Zondlo, H. Finklea, O. Demircan, M. Gong, X. Liu, Journal of Power Sources 193 (2009) 739–746.
[2] C. Xu, J. Zondlo, M. Gong, X. Liu, Journal of Power Sources 196 (2011) 116–125.
[3] J.P. Trembly, Investigation into the Effects of Trace Coal Syngas Species on the Performance of Solid Oxide Fuel Cell Anodes, PhD. Dissertation, The Russ College of Engineering and Technology of Ohio University, 2007.
[4] O.A. Marina, C.A. Coyle, E.C. Thomsen, D.L. Edwards, G.W. Coffey, L.R. Pederson, Solid State Ionics 181 (2010) 430–440.
[5] E. Kostiner, J.R. Rea, Inorganic Chemistry 13 (12) (1974) 2876–2880.
[6] M. Yousuf, P.C. Sahu, H.K. Jajoo, S. Rajagopalan, K. Govinda Rajan, Journal of Physics F 16F (1986) 373–378.
[7] T. Swanson, Natl. Bur. Stand. (U.S.) Circ. No., vol. VI, 539, 1955, 3 pp.
[8] M. Yashima, S. Sasaki, M. Kakihana, Acta Crystallographica Section B 50 (December) (1994) 663–672.
[9] J.F. Moulder, W.F. Stickle, P.E. Sobol, K.D. Bomben, Handbook of X-ray Photoelectron Spectroscopy, Physical Electronics, Eden Prairie, MN, 1995.
[10] Y. Wang, D.J. Asunskis, P.M.A. Sherwood, Surface Science Spectra 9 (1) (2002) 91.
[11] S. Zha, Z. Cheng, M. Liu, Journal of the Electrochemical Society 154 (2) (2007) B201–B206.
[12] H. Ishii, K. Asakura, T. Ohta, Y. Kitajima, H. Kuroda, Japanese Journal of Applied Physics 32 (Suppl. 32-2) (1993) 368–370.
[13] K. Asakura, H. Ishii, S. Konishi, Y. Kitajim, T. Ohta, H. Kurod, Physica B 208–209 (1995) 465–466.
[14] M. Gong, D. Bierschenk, J. Haag, K.R. Poeppelmeier, S.A. Barnett, C. Xu, J.W. Zondlo, X. Liu, Journal of Power Sources 195 (2010) 4013–4021.
[15] J.P. Trembly, R.S. Gemmen, D.J. Bayless, Journal of Power Sources 163 (2007) 986–996.
[16] J.P. Trembly, R.S. Gemmen, D.J. Bayless, Journal of Power Sources 171 (2007) 818–825.
[17] O.A. Marina, L.R. Pederson, C.A. Coyle, D.L. Edwards, Y. Chou, C.N. Cramer, Journal of Power Sources 196 (2011) 636–643.
[18] A. Martinez, K. Gerdes, R. Gemmen, J. Poston, Journal of Power Sources 195 (2010) 5206–5212.